Chinese Journal of
POLYMER SCIENCE

ARTICLE

https://doi.org/10.1007/s10118-021-2513-3
Chinese J. Polym. Sci. **2021**, *39*, 425–440

Robust and Self-healable Antibiofilm Multilayer Coatings

Chao Zhou[a,†*], Jun-Tao Zhou[a,†], Cheng-Ju Sheng[a], Dicky Pranantyo[b], Yan Pan[a], and Xiao-Jia Huang[a]

[a] *Institute of Biomedical Engineering and Health Sciences, Changzhou University, Changzhou 213164, China*
[b] *Department of Chemical and Biomolecular Engineering, National University of Singapore, 117585, Singapore*

Electronic Supplementary Information

Abstract The infection induced by implantation of biomedical materials may result from the biofilm formation after bacteria attachment. Hence, the antibiofilm surface coating represents a novel technique to improve the antibacterial activity of biomedical materials. The traditional antibiofilm surface coatings exhibited some disadvantages and provided a limited service life. In this work, we used polyethyleneimine grafted 3-maleimidopropionic acid (PEIM) and poly(acrylic acid) grafted 2-furfurylamine (PAAF) to achieve robust and self-healable crosslinked multilayer coatings, employing Layer-by-Layer (LbL) self-assembly technique and Diels-Alder reaction. Then, thiol-terminated poly((3-acrylamidopropyl) trimethylammonium chloride) (PAMPTMA-SH) was grafted onto the crosslinked multilayer coating by thiol-ene click reaction to form a novel multilayer coating $(PEIM/PAAF)_{10}$-PAMPTMA. We found that this coating showed robust and self-healable activity, and significantly inhibited the bacterial growth and biofilm formation after infection with *Escherichia coli* (*E. coli*) and *Staphylococcus aureus* (*S. aureus*) by *in vitro* and *in vivo* assays for 120 h. In addition, the multilayer coating did not induce significant hemolysis or affect the cell viability of red blood cells. *In vivo* studies also showed that $(PEIM/PAAF)_{10}$-PAMPTMA coating efficiently blocked the infiltration of inflammatory cells and gene expression in the mouse skin challenged with *E. coli* or *S. aureus*. Taken together, these results showed that the prepared multilayer coating exhibited strong antibiofilm activity and provided a new strategy for the application of highly efficient antibiofilm surface coating of biomedical materials.

Keywords Layer-by-Layer assembly; Diels-Alder reaction; Self-healable; Antibiofilm coating; Thiol-ene click reaction

Citation: Zhou, C.; Zhou, J. T.; Sheng, C. J.; Pranantyo, D.; Pan, Y.; Huang, X. J. Robust and self-healable antibiofilm multilayer coatings. *Chinese J. Polym. Sci.* **2021**, *39*, 425–440.

INTRODUCTION

Microbial adhesion onto device/implant surfaces and formation of bacterial biofilms associated infections have become one of the challenging threats to biomedical devices in hospitals and implants in patients.[1–3] Therefore, many scientists developed various methods for preparing antibacterial or antifouling surface coatings such as exclusion steric repulsion,[4,5] electrostatic repulsion,[6,7] low surface energy,[8,9] biocide releasing,[10–13] and contact-active antimicrobial.[14–18] However, the occurrence of scratches and partial exfoliation is inevitable during the long-term application, leading to the surface devastation and failure of the biomedical devices and implants.[19–21] Accordingly, the self-healing surface coating has been of great importance in improving the stability and durability of functional antibacterial coatings in long-term applications.[22–24] As viewed from the predominant molecular mechanisms involved in the healing processes on functional polymer materials, the reported achievements consisted of two modes: (i) physical interactions (including hydrogen bond, hydrophobic interaction, host-guest interaction, crystallization, polymer-nanocomposite interaction, and multiple intermolecular interaction), and (ii) chemical interactions (including phenylboronate complexation, disulfide bonds, imine bonds, acrylhydrazone bonds, reversible radical reaction and Diels-Alder reaction).[25–28]

Layer-by-Layer (LbL) self-assembly technology is one of the convenient and flexible methods for the fabrication of self-healing polymer coatings on various substrates. LbL self-assembly is carried out through high diffusion by alternately depositing oppositely charged polyelectrolytes and generating high mobility of polyelectrolytes multilayer onto a charged substrate surface when subjected to external stimuli.[29–32] However, the instinct of loose structures and weak non-covalent bonds between polyelectrolyte layers makes the multilayers separated from top to bottom of the surface coatings during the long-term application. In order to prevent top-down degradable multilayer, some scientists investigated crosslinked multilayers by condensation reaction[33,34] or click chemistry[35] to control the multilayer degradation rate. In these cases, the high temperature and long-time reaction of condensation reaction or high crosslinking density of click chemistry made the assembled multilayer mobility difficult, and thus the self-healing surface coating could not be achieved. Therefore, it seemed to be a contradiction between

* Corresponding author, E-mail: zhouchao@cczu.edu.cn
† These authors contributed equally to this work.
Received July 28, 2020; Accepted October 5, 2020; Published online October 26, 2020

© Chinese Chemical Society
Institute of Chemistry, Chinese Academy of Sciences
Springer-Verlag GmbH Germany, part of Springer Nature 2020

robust and self-healing properties for the surface coating.

In this work, we developed a method for fabricating robust and self-healable antibiofilm surface coating. Firstly, polyethyleneimine (PEI) grafted 3-maleimidopropionic acid (PEIM) as a positive layer and poly(acrylic acid) (PAA) grafted 2-furfurylamine (PAAF) as a negative layer were used to fabricate robust and self-healable surface coating by LbL self-assembly technique and Diels-Alder reaction. Then thiol terminated poly((3-acrylamidopropyl) trimethylammonium chloride) (PAMPTMA-SH) as the antibacterial polymer prepared by supplemental activator and reducing agent atom transfer radical polymerization (SARA ATRP) was grafted onto the oxynorbornene crosslinking group formed from Diels-Alder reaction of the multilayer coating by thiol-ene click reaction (Scheme 1). The as-prepared multilayer coating exhibited not only robust and self-healable properties, but also long-term antibiofilm efficacy, which could be applied in biomedical devices.

EXPERIMENTAL

Materials

Dopamine hydrochloride (DA, 99%), 2-hydroxyethyl disulfide (99%) and (3-acrylamidopropyl) trimethylammonium chloride (AMPTMA, 75%) were purchased from Sigma Aldrich (St. Louis, MO, USA); triethylamine (TEA, 99%), α-bromoisobutyryl bromide (BiBB, 98%), $CuBr_2$ (97%), tris base (Trizma base, Pharma grade), 4-dimethylaminopyridine (DMAP, 99%), methanol (99%),

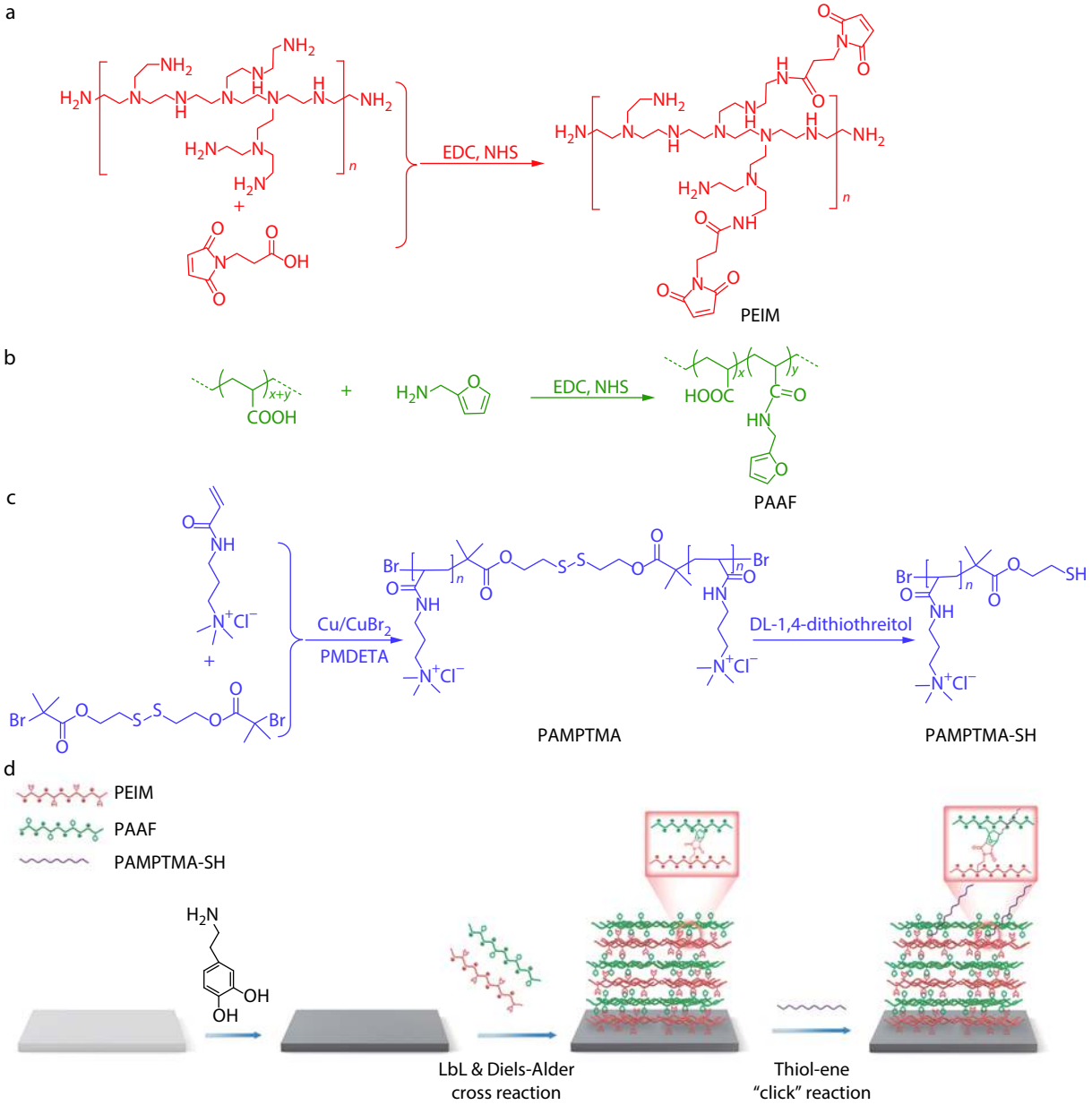

Scheme 1 Procedure of (a) PEIM, (b) PAAF, (c) PAMPTMA-SH, and (d) robust and self-healable antibiofilm surface coating.

https://doi.org/10.1007/s10118-021-2513-3

N,N,N′,N″,N‴-pentamethyldiethylenetriamine (PMDETA, 99%), dimethyl sulfoxide (DMSO), DL-1,4-dithiothreitol (DTT, 98%), 2-furfurylamine (99%), maleic anhydride (MAH, 99%), *β*-alanine (99%), tetrahydrofuran (THF, 99%), *N*-hydroxysuccinimide (NHS, 99%), 1-(3-dimethylaminopropyl)-3-ethylcarbodiimide hydrochloride (EDC, 99%), and glutaraldehyde (3%) were purchased from Aladdin (Shanghai, China). PEI (M_n=1.0×10^4) and PAA (M_n=1.0×10^5) were purchased from Macklin (Shanghai, China); copper wire (Cu(0), *d*=1 mm) was washed with HCl, rinsed with methanol, and dried under a stream of N_2 before use. Dulbecco's phosphate buffered saline (PBS) was purchased from Sigma-Aldrich; Dulbecco's Modified Eagle's Medium, 3-(4,5-dimethylthiazol-2-yl)-2,5-diphenyltetrazolium bromide (MTT), L13152 LIVE/DEAD® Bac Light TM Bacterial Viability Kit were purchased from Thermo Fisher Scientific; Triton X-100 (0.3%) was purchased from SAIES, China; phalloidin-TRITC and 4′,6-diamidino-2-phenylindole (DAPI) were purchased from Sigma-Aldrich; 4% paraformaldehyde was purchased from Boster Biological Technology Co.

Synthesis of PAMPTMA-SH by SARA ATRP

Firstly, we synthesized disulfide initiator bis[2-(2-bromoisobutyryloxy)ethyl] disulfide (BiBOEDS) as bifunctional atom transfer radical polymerization (ATRP) initiator according to the previous paper.[36] Secondly, BiBOEDS (0.036 g, 0.08 mmol), AMPTMA (3.97 mL, 16 mmol), $CuBr_2$ (5.40 mg, 0.024 mmol) and PMDETA (5 μL, 0.024 mmol) were dissolved in 6 mL of a 50/50 volume mixture of water and methanol. A magnetic stirring bar and copper wire (1.00 g, *d*=1.00 mm) were added to the Schlenk flask, sealed with rubber stopper and deoxygenated with N_2 under three freeze-vacuum-thaw cycles. Then the reaction was carried out at 50 °C and stirred at 940 r/min under nitrogen condition for 24 h. Finally, the reaction mixture was dialyzed against deionized water (DI H_2O) for 3 days and disulfide poly((3-acrylamidopropyl) trimethylammonium chloride) (DSPAMPTMA) was obtained after freeze drying. Proton nuclear magnetic resonance (^{1}H-NMR) (400 MHz, D_2O, *δ*, ppm): 1.07 (s, 12 H, $-C\underline{H}_3$), 1.92 (s, 148H, $-C\underline{H}_2-$), 3.05 (s, 451H $-N^+-C\underline{H}_3$), 3.72 (s, 145H, $N^+-C\underline{H}_3$), 3.20 (s, 79H, $NH-C\underline{H}_2-$), 3.45 (s, 77H, $-C\underline{H}_2-N^+$).

The as-prepared DSPAMPTMA disulfide was dissolved in 20 mL of THF and purged with N_2 for 30 min. DTT (0.77 g, 5 mmol) was introduced into mixture solution. The mixture was stirred for 24 h under N_2 condition at 50 °C. The resulting PAMPTMA-SH solution was dialyzed against DI H_2O for 2 days. The dry PAMPTMA-SH polymer was obtained after freeze drying.

Synthesis of PAAF

PAAF was synthesized by dissolving PAA (1 g, 0.01 mmol) in 50 mL of 1×PBS (pH=7.4). NHS (0.32 g, 2.80 mmol) and EDC (0.54 g, 2.80 mmol) were added in the mixture and it was stirred for 6 h at 37 °C. Then, 2-furfurylamine (0.27 g, 2.80 mmol) was added dropwise into the above mixture. The reaction mixture was stirred for 48 h at 37 °C and dialyzed (7 kDa MWCO) against 0.1 mol/L NaCl for 2 days, followed by further dialysis against DI H_2O for 2 days. The product was obtained after freeze drying. ^{1}H-NMR (400 MHz, D_2O, *δ*, ppm): 2.32 (s, 347H, $-C\underline{H}_2-$), 6.18 (s, 2H, $-C=C\underline{H}-C\underline{H}=C-$).

Synthesis of PEIM

3-Maleimidopropionic acid was synthesized as previously described.[37] PEIM was synthesized by dissolving branched PEI (1 g, 0.10 mmol) in 50 mL of 1×PBS (pH=7.4). NHS (0.50 g, 4.30 mmol) and EDC (0.82 g, 4.30 mmol) were added in the mixture and it was stirred for 6 h at 37 °C. Then 3-maleimidopropionic acid (0.73 g, 4.30 mmol) was added dropwise into the above mixture. The reaction mixture was stirred for 48 h at 37 °C and dialyzed (4 kDa MWCO) against 0.1 mol/L NaCl for 2 days, followed by further dialysis against DI H_2O for 2 days. The product was obtained after freeze drying. ^{1}H-NMR (400 MHz, D_2O, *δ*, ppm): 2.09–3.57 (m, 67H, $-C\underline{H}_2-$), 5.94 (s, 2H, $-C\underline{H}=C\underline{H}-$).

Fabrication of Self-healing Surface Coating by Layer-by-layer Self-assembly and Diels-Alder Reaction

Firstly, stainless steel (SS) slides (*d*=10 mm) were washed with ethanol and DI H_2O three times in ultrasonic bath and dried with N_2; secondly, the SS slides were pre-treated with piranha solvent ($V(H_2SO_4)$:$V(H_2O_2)$=7:3) for 40 min, washed with DI H_2O, and dried with N_2; thirdly, the pre-treated SS slides were immersed into Tris-HCl solution (pH=8.5, 10 mmol/L), which contained 4 mg/mL DA, and strongly stirred for 24 h at 37 °C until the SS slides showed an evident color change from metallic to dark brown. The SS coated poly(dopamine) (SS-PDA) slides were then rinsed with DI H_2O and dried overnight in a vacuum dryer at 50 °C.

With the as-prepared PEIM as positive charge layer, PAAF as negative charge layer, the PEIM/PAAF layers coated onto SS-PDA slides were fabricated by LbL self-assembly. The SS-PDA slides were alternately immersed in aqueous solutions of PEIM (1 mg/mL, pH=8.4) and PAAF (1 mg/mL, pH=3.5) for 10 min each time, followed by rinsing three times for 1 min each in DI H_2O baths, respectively. By repeating the above deposition and rinsing steps in a cyclic fashion, multilayer coating $(PEIM/PAAF)_{10}$ with 10 deposition cycles can be fabricated. The drying step with N_2 was only conducted after depositing the last layer. Diels-Alder reaction of multilayer coating $(PEIM/PAAF)_{10}$ on SS-PDA slides surface was carried out in oven at 50 °C for 4 h.

The $(PEI/PAA)_{10}$ multilayer coatings as control samples were fabricated on SS-PDA slides surface in the same way with the $(PEIM/PAAF)_{10}$ slides, but without crosslinking procedure.

Fabrication of Antibiofilm Surface Coating Based on $(PEIM/PAAF)_{10}$ Multilayer by Thiol-ene Click Reaction

The as-prepared PAMPTMA-SH (50 mg) was dissolved in DI H_2O to form the concentration of 3 mg/mL, containing 0.5% UV initiator (IRGACURE 2959). SS-PDA slides coated with $(PEIM/PAAF)_{10}$ multilayer coating were immersed into the polymer solution under N_2. The thiol-ene click reaction was carried out under UV reaction (wavelength 365 nm, MXGain-LAB40A, Shanghai, China) for 15 min at 25 °C. Finally, the $(PEIM/PAAF)_{10}$-PAMPTMA coated SS slide was washed by DI H_2O three times and dried by N_2.

Characterization

Functional groups of polymers were characterized by ^{1}H-NMR (AVANCE III 400 MHz, Bruker) using the solvent signal for

calibration and Fourier transform infrared spectrometry (FTIR) (Nicolet-460, Thermo Fisher). The molecular weight of polymers was characterized by gel permeation chromatography (GPC) measurements, performed on Waters GPC system, equipped with a Waters 1515 isocratic HPLC pump, a Waters 717 plus Autosampler injector, and a Waters 2414 refractive index detector, using water as the eluent at a flow rate of 1.0 mL/min.

The surface structures of SS and modified SS slides were characterized by X-ray photoelectron spectroscopy (XPS) measurements, carried out on a Kratos AXIS Ultra HSA spectrometer equipped with a monochromatized Al Kα X-ray source (1468.6 eV photons). Static water contact angles were measured using JC2000D1 goniometer (Powereach, China) and employing the sessile drop method at room temperature. Surface morphology of LbL self-assembly multilayer coatings on SS slides was characterized by field emission scanning electron microscopy (FE-SEM) (Zeiss Sigma 500, Germany). Thickness of LbL self-assembly multilayer coatings on SS slides was measured by spectroscopic ellipsometry (VASE J. A. Woollam). The surface charge of multilayers on surfaces was characterized by surface zeta potential measurement (Anton Paar Electro Kinetic Analyzer).

Quartz crystal microbalance (QCM) (QCM-Z500) measurements were carried out with an Au-coated resonator. The crystal was mounted in a fluid cell with one side exposed to the solution. A measurement of LbL deposition was initiated by switching the liquid exposed to the resonator. Then, PEI and PAA solutions were alternately introduced with buffer rinsing for 10 min. Both PEI and PAA were 1 mg/mL in DI water and injected into the fluid cell at a rate of 200 μL/min to fabricate multilayer coating $(PEI/PAA)_{10}$. The QCM measurement of $(PEIM/PAAF)_{10}$ followed the same procedure.

The Stability and Degradation of Multilayer Coatings

The stability of surface multilayer coatings was measured by UV-Vis absorption spectra (Shimadzu UV-2450 spectrophotometer, Japan) and surface nanoindentation test instrument (Bruker, Hysitron TI 980 TriboIndenter, U.S.). Firstly, the multilayers were coated onto the quartz glass and immersed in PBS at 37 °C for different time periods, and then the multilayer coated quartz glass was dried by N_2 and measured by UV-Vis absorption spectra in the wavelength range from 190 nm to 700 nm. Secondly, the stiffness of surface multilayer coatings was tested by nanoindentation test instrument according the reported method.[38]

Self-healing Procedure of Multilayer Coatings on SS Slide

The self-healing process of scratches (made by a scalpel) on the surface of each sample was conducted in open air at room temperature (25 °C). The morphologies of samples during the self-healing process were observed by an atom force microscope (AFM) with tapping mode (Bruker, U.S.) and a polarizing optical microscope (Nikon, ECLIPSE E200).

In Vitro Antimicrobial Activity of Multilayer Coatings on SS Slide

SS and modified SS slides (d=10 mm, previously washed with water then dried and UV sterilized for 1 h) were put into a 24-well plate, and added with 1 mL of 10^6 CFU/mL for *E. coli* and 10^7 CFU/mL for *S. aureus* bacteria suspensions into each well, respectively (LB for *E. coli* and MHB for *S. aureus*). The plate was incubated at 37 °C for 24, 72 and 120 h, respectively (added with fresh medium every two days). Each sample was washed gently thrice with PBS buffer to remove unattached bacteria. Each sample was then placed in 10 mL of PBS buffer. Then the slides were placed in ultrasonicator bath for 30 min to remove the attached bacteria from the surface. CFU number was counted by dilution of the stripped bacteria suspension in PBS and culture on LB Agar and MHA plates, respectively. Log reduction was calculated using Eq. (1):

$$\text{Number of log reduction} = \log_{10}\left[\text{CFU}_{\text{control}}/\text{CFU}_{\text{sample}}\right] \quad (1)$$

Fluorescence Microscopy

SS and modified SS slides (d=10 mm, previously washed with water then dried and UV sterilized for 1 h) were put into a 24-well plate, respectively, and then 1 mL of MC3T3-E1 suspension was seeded in each well with a density of 1.0×10^4 cells/mL. After 24 h incubation in growth medium, the samples were rinsed carefully with PBS buffer solution. Then 4% paraformaldehyde was used to fix cells for 10 min. After SS and modified SS slides were washed with PBS three times (5 min each wash), the cells were permeabilized with 0.5% Triton X-100 in PBS for 5 min, and the microfilaments were labeled with 1 mg/mL phalloidin-TRITC for 30 min. The cells were treated with 2 mg/mL DAPI for 5 min to stain cell nuclei, and finally all the stained samples were rinsed with DI H_2O thoroughly. Cell images were recorded on an inverted fluorescence microscope (EVOS™ FL Imaging System AMF4300, ThermoFisher, U.S).

SS and modified SS slides (d=10 mm, previously washed with water then dried and UV sterilized for 1 h) were put into a 24-well plate, and added with 1 mL of 10^6 CFU/mL for *E. coli* and 10^7 CFU/mL for *S. aureus* bacteria suspensions into each well, respectively. The plate was incubated at 37 °C for 120 h. SS and modified SS slides were washed gently thrice with PBS buffer to remove unattached bacteria. Stain containing L13152 LIVE/DEAD® Bac Light TM Bacterial Viability Kit was used by consulting the manufacturer's protocol. Stain solution (40 μL, the final concentration of each dye will be 6 μmol/L SYTO 9 stain and 30 μmol/L propidium iodide) was added and spread on each sample and incubated in the dark for 15 min before examination under a fluorescence microscope. Fluorescence imaging was done with 480/500 nm filter for SYTO 9 stain and 490/635 nm filter for propidium iodide in the microscope optical path by Zeiss LSM 710 for the live/dead bacteria imaging.

Biofilm Morphology Check under FE-SEM

SS and modified SS slides (d=10 mm, previously washed with water then dried and UV sterilized for 1 h) were put into a 24-well plate, and added with 1 mL of 10^6 CFU/mL for *E. coli* and 10^7 CFU/mL for *S. aureus* bacteria suspensions (LB for *E. coli* and MHB for *S. aureus*) into each well, respectively. The plate was incubated at 37 °C for 120 h. SS and modified SS slides were washed gently thrice with PBS buffer to remove unattached bacteria. Each sample was immersed into 2 mL of 3% glutaraldehyde in PBS and refrigerated at 4 °C overnight. The samples were dehydrated with a graded concentration series of ethanol/water mixtures (25%, 50%, 75%, 100%). Dehydrated samples were further dried under nitrogen before characterized by FE-SEM.

Hemolytic Assays of Multilayer Coatings on SS Slide

Fresh human blood (5 mL) was collected from a healthy donor (age 25, male). Erythrocytes were separated by centrifugation at 1200 r/min for 10 min, washed thrice with PBS buffer, and diluted to a final concentration of 5 vol%. SS and modified SS slides (d=10 mm, previously washed with water then dried and UV sterilized for 1 h) were immersed into 1 mL of erythrocytes stock placed in a 24-well cell culture plate. All measurements were performed in triplicate. The plate was incubated at 37 °C for 1 h with shaking at 200 r/min. Subsequently, the slides were centrifuged at 1500 r/min for 10 min. Aliquots (100 μL) of supernatant were transferred to a new 96-well plate. Hemolytic activity was determined by absorbance measurement at 540 nm with infinite F50 TECAN plate reader. Triton X-100 (0.3% in PBS), which was able to lyse red blood cells (RBCs) completely, was used as positive control while diluted erythrocytes (5 vol% in PBS) were used as negative control. The hemolysis percentage was calculated using Eq. (2):

$$\text{Hemolysis} = \left[\text{OD}_{\text{sample}} - \text{OD}_{\text{negative}}\right] / \left[\text{OD}_{\text{positive}} - \text{OD}_{\text{negative}}\right] \times 100\% \quad (2)$$

In Vitro Cytocompatibility Assay of Multilayer Coatings on SS slides

Firstly, SS and modified SS slides (d=10 mm SS, previously washed with water then dried and UV sterilized for 1 h) were immersed into PBS for 24 h at room temperature; then 100 μL of 10^5 cells/well MC3T3-E1 cell suspension in supplemented Dulbecco's Modified Eagle's Medium (DMEM with 10% FBS and 1% penicillin-streptomycin) and 100 μL of extracted liquid from the slides were seeded in a 96-well cell culture plate and incubated for 24 h at 37 °C in 5% CO_2; the blank control was replaced with 100 μL of PBS. After 24 h, 20 μL of MTT (5 mg/mL) was added to each well followed by another 4 h of incubation. The MTT-DMEM solution was discarded, and 150 μL of dimethyl sulfoxide (DMSO) was added to each well and shaken for 15 min. Absorbance values (ODs) were measured at 570 nm using an infinite F50 TECAN plate reader. Cell viability was calculated using Eq. (3):

$$\text{Cell viability} = \left[\text{OD}_{\text{sample well}}\right] / \left[\text{OD}_{\text{control well}}\right] \times 100\% \quad (3)$$

In Vivo Antimicrobial Activity of Multilayer Coatings on SS Slide

E. coli (10^6 CFU/mL, 10 μL) and *S. aureus* (10^6 CFU/mL, 10 μL) were respectively spotted on the SS slide (d=5 mm) or multilayer coating $(\text{PEIM/PAAF})_{10}$-PAMPTMA on SS-PDA (d=5 mm) and dried for 15 min. ICR mice (five weeks old female) were purchased from SPF (Beijing Biotechnology Co., Ltd., China). Mice were divided into four groups: SS slide and coated SS slide for *E. coli* as well as SS slide and coated SS slide for *S. aureus*, and each group of samples had five replicates. All animals were housed under specific pathogen-free conditions (24 °C, 12 h light/12 h dark cycles and 50% humidity) with free access to food pellets and tap water. All mice's back were shaved and sterilized to generate a 0.5 cm × 1 cm incision to the spine on each side. The slide was implanted into each incision respectively and the incisions were closed with a single 0/6 vicryl stitch subsequently. After 120 h, the implant slides were taken out, and then the incision of skin tissue was cut off in 1 cm × 1 cm square. Then the harvested skin tissue was cut into several pieces and one of pieces was placed in 1 mL of PBS. The mixture was vigorously shaken for 10 min to remove all the bacteria from skin tissue. CFU number was counted by dilution of the stripped bacteria suspension in PBS and culture on LB Agar for *E. coli* and MHA for *S. aureus*, respectively. Log reduction was calculated using Eq. (1).

Part of the harvested tissues were fixed in 4% phosphate-buffered paraformaldehyde for 12 h and embedded in paraffin. Serial sections (5 μm thick) were cut from the paraffin embedded blocks and underwent H&E staining. Photographs were analyzed using a polarizing optical microscope (Nikon, ECLIPSE E200) from three randomly selected views of each specimen, respectively.

RNA Extraction and Real-time RT-PCR of mRNA

The mRNA was extracted by TRIzol reagent (Takara, Japan) according to the manufacturer's protocol from part of the tissue. Then, 1 μg of mRNA was reversely transcribed to cDNA with Fast Quant RT Super Mix (TIANGEN, China) by Veriti 96 well thermal cycler (Applied Biosystems, USA). Real-time reverse transcription polymerase chain reaction (RT-PCR) analysis was performed by using the SYBR Premix Ex Taq II kit (Takara, Japan) and tested by Step One Plus real-time PCR system (Applied Biosystems, USA). Cyclophilin A (PPIA) was used as the internal control for quantitation of the inflammation expressed mRNA (TNF-α, IL-6, IL-1β in Table S1 in the electronic supplementary information, ESI). The setting of program was 95 °C for 10 min, 40 cycles of 95 °C for 15 s, and 60 °C for 1 min.

RESULTS AND DISCUSSION

Synthesis of Functional Polymers

DSPAMPTMA as the antibacterial polymer was synthesized by SARA ATRP.[39,40] GPC was used to determine the molecular weights and polydispersity (PDI) of the polymers in aqueous solution. From GPC result in Fig. 1, the estimated M_n of DSPAMPTMA was 14000 g/mol with a PDI of 1.4. DSPAMPTMA was reduced to PAMPTMA-SH using DTT, and the molecular weight of PAMPTMA-SH decreased to 8000 g/mol (PDI=1.4) (Fig. 1).

PAAF was synthesized by amination reaction of PAA and 2-furfurylamine with the aid of NHS and EDC.[41] From ^{1}H-NMR in Fig. S1(b) (in ESI), a weak signal at 6.18 ppm corresponding

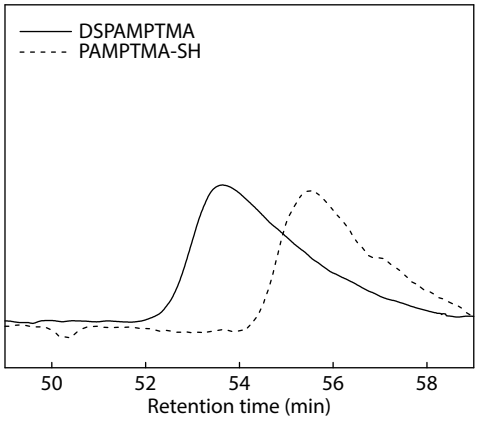

Fig. 1 GPC curves of DSPAMPTMA and PAMPTMA-SH.

https://doi.org/10.1007/s10118-021-2513-3

to double bond protons of furan groups confirmed that the 2-furfurylamine groups were grafted onto PAA backbone successfully; furan substitution ratio of the area under the furan proton signal (6.18 ppm) to the area under the signal for ethylene group protons on PAA (2.32 ppm) determined that the 16 furan groups were grafted onto per PAA polymer chain. FTIR spectra of PAA and PAAF are shown in Figs. 2(a) and 2(b). PAA exhibited a characteristic band in the region of 1700 cm^{-1} due to C=O stretching vibration. A new band at 1631 cm^{-1} in PAAF assigned to O=C—N—H was attributed to N—H bending vibration and also confirmed that 2-furfurylamine was grafted onto PAA successfully.

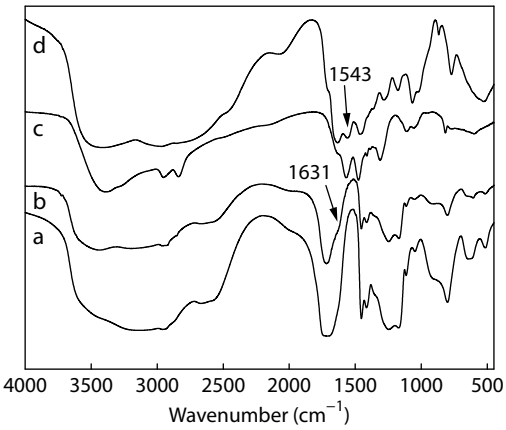

Fig. 2 FTIR spectra of (a) PAA, (b) PAAF, (c) PEI, (d) PEIM.

PEIM was prepared by a similar procedure to PAAF.[42] In order to prevent Michael addition between amine of PEI and maleimidopropionic acid , the priority amide formation of PEI and 3-maleimidopropionic acid was carried out at 37 °C, compared with Michael addition.[43] The signal in ^{1}H-NMR spectra in Fig. S1(c) (in ESI) at 5.94 ppm corresponded to the double bond of the maleimide proton; maleimide substitution ratio of the area under the signal for maleimide proton (5.94 ppm) to the area under the signals for ethylene group protons on PEI (2.09–3.57 ppm) determined that the 13 maleimide groups were grafted onto per PEI polymer chain. FTIR spectra of PEI and PEIM are shown in Figs. 2(c) and 2(d). PEI exhibited two characteristic bands in the region of 3500–3300 cm^{-1} due to N—H stretching vibration. For PEIM, a new band, belonging to C=O stretching vibration, appeared at 1543 cm^{-1}. It was concluded that the 3-maleimidopropionic acid groups were grafted onto the PEI backbone successfully.

Polyelectrolyte Multilayer Coatings by LbL Self-assembly

Firstly, acid treated SS coated poly(dopamine) (SS-PDA) was prepared by 4 mg/mL DA in Tris-HCl solution, and then PEIM as positive charge layers was coated onto SS-PDA. There was Schiff-base formation between amine group of PEIM and PDA carbonyl groups of SS-PDA surface.[44] PAAF as negative charge layers was coated onto PEIM layer. Multilayer coating $(PEIM/PAAF)_{10}$ with 10 deposition cycles can be fabricated by LbL self-assembly. Finally, the multilayer coating was crosslinked by Diels-Alder reaction at 50 °C for 4 h. Similarly, traditional multilayer coating $(PEI/PAA)_{10}$ without crosslinking procedure as control was fabricated on SS-PDA slides surface in the same way as $(PEIM/PAAF)_{10}$.

From XPS wide scans of SS and modified SS slides in Fig. 3(a), N1s peak appeared on SS-PDA coating $(PEI/PAA)_{10}$, $(PEIM/PAAF)_{10}$, and $(PEIM/PAAF)_{10}$-PAMPTMA multilayer coatings, as compared with SS slide. Because SS slide was covered by PDA coatings, Fe content decreased on SS-PDA substrate surface, while N content increased, as listed in Table 1. The C1s core level spectra of the modified SS slides also showed the O—C=N peak at 286.0 eV in Figs. 3(b)–3(f), compared with SS slide. The N1s core level spectra of PDA coating showed peaks at 400.5 and 399.6 eV, corresponding to its predominant secondary amine groups of indole and imine functionalities (Fig. 3g).[45] Moreover, $(PEI/PAA)_{10}$ and $(PEIM/PAAF)_{10}$ multilayer showed a new peak at 401.5 eV, corresponding to primary amine of PEI and PEIM. The intensity of the secondary amine at 400.5 eV was also enhanced. $(PEIM/PAAF)_{10}$-PAMPTMA was constructed using cationic polymer (PAMPTMA-SH) grafted onto the $(PEIM/PAAF)_{10}$ multilayer by thiol-ene click reaction. A new N1s core level spectra peak appeared at 402.5 eV, which corresponded to —$\underline{N}^+$H— of $(PEIM/PAAF)_{10}$-PAMPTMA in Fig. 3(g). S2p peak at 164.1–169.0 eV appeared in wide scan of $(PEIM/PAAF)_{10}$-PAMPTMA and its S2p core level spectra showed strong signal in Fig. 3(h), confirming that PAMPTMA-SH was grafted onto $(PEIM/PAAF)_{10}$ multilayer coating successfully.

Physical Properties of Multilayer Coatings

After fabrication of the LbL multilayer coatings onto SS-PDA slides, we compared the difference of physical properties between traditional multilayer $(PEI/PAA)_{10}$ and novel multilayer $(PEIM/PAAF)_{10}$. Firstly, the wettability of $(PEI/PAA)_{10}$ and $(PEIM/PAAF)_{10}$ was evaluated by static water contact angle analysis (Fig. 4a). The SS substrate was found to be hydrophilic, with a contact angle of 48°±10°. The contact angle decreased to 29°±2° after coating PDA onto SS. Subsequently, PEI layer was coated, and the contact angle was changed to 35°±5°. After the PAA layer self-assembled, the contact angle decreased to 0°±1° in a short time, which is because that the contact angle shows a distinct time dependence with the droplets in PAA out-most layers.[46] For the $(PEIM/PAAF)_{10}$ multilayer coating, the contact angle was changed to 20°±5° after PEIM layer was coated, and the contact angle was still 0°±1° after PAAF layer was covered.

Afterwards, the thickness of multilayer $(PEI/PAA)_{10}$ increased rapidly in a nearly linear manner (Fig. 4b) as revealed by QCM, while the thickness of $(PEI/PAA)_{10}$ reached up to 1300 nm. However, the thickness of $(PEIM/PAAF)_{10}$ increased in a slow but almost linear way with increasing numbers of coating deposition cycles, and reached a maximum thickness of 500 nm. This is because PAA contained ~5% negatively charged carboxylate groups in pH 3.5 aqueous solution.[47] However, PAAF had fewer carboxylate groups than PAA due to PAA grafting furan groups. Similarly, PEIM provided fewer primary and secondary amine groups than PEI due to polymer chain grafting maleimide groups. Carboxylate groups of PAA could have stronger electrostatic interactions with protonated primary and secondary amine groups of PEI in $(PEI/PAA)_{10}$ than the interaction between PAAF and PEIM in

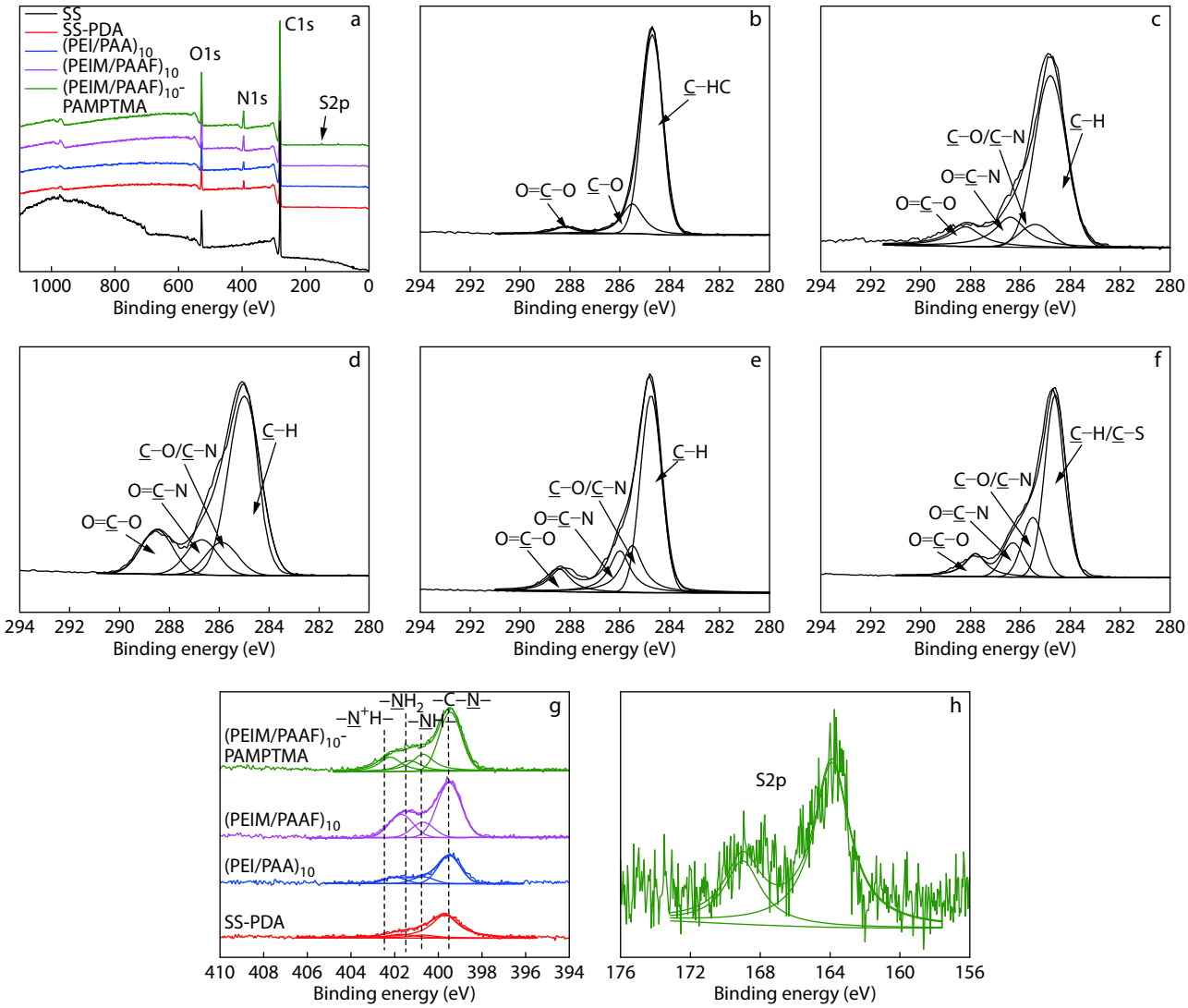

Fig. 3 (a) Wide scan spectra; C1s core level spectra of (b) SS, (c) SS-PDA coating, (d) $(PEI/PAA)_{10}$ multilayer coating, (e) $(PEIM/PAAF)_{10}$ multilayer coating, and (f) $(PEIM/PAAF)_{10}$-PAMPTMA multilayer coating; (g) N1s core level spectra of SS slide and multilayer coatings on SS slide; (h) S2p core level spectra of $(PEIM/PAAF)_{10}$-PAMPTMA.

Table 1 Surface characterization of multilayer coatings.

Coating samples	XPS atomic percent (%) Fe:C:N:S:Br	Layer thickness (nm)	Surface zeta potential (mV)
SS	3.13:92.87:4.01:–:–	6.18±0.83	−37.80±2.83
SS-PDA	2.74:89.07:8.19:–:–	29.82±3.38	−50.22±3.21
$(PEI/PAA)_{10}$	1.88:90.72:7.40:–:–	50.22±2.73	−56.10±4.79
$(PEIM/PAAF)_{10}$	0.40:90.65:8.95:–:–	44.11±5.94	−42.17±2.10
$(PEIM/PAAF)_{10}$-PAMPTMA	0.23:86.64:12.6:0.41:0.12	52.84±5.71	3.80±1.36

$(PEIM/PAAF)_{10}$. The thicknesses of $(PEI/PAA)_{10}$ and $(PEIM/PAAF)_{10}$ were 50.2 and 40.1 nm, respectively, as measured by spectroscopic ellipsometry, smaller than the QCM measuring results. This is because wet and swelled multilayer coatings were measured by QCM, while dry multilayer coatings were measured by spectroscopic ellipsometry. The surface roughness and morphology of multilayer coatings were characterized by AFM and FE-SEM as shown in Fig. 4(c) and Fig. 5, respectively. The roughness of SS-PDA slide coated with LbL multilayer coatings decreased as compared to SS slide and SS-PDA slide, because the multilayer coatings absorbed water and covered the substrate uniformly. The surface morphology characterization by FE-SEM also confirmed that LbL multilayer coatings were uniform on the SS slide.

The Stability of Multilayer Coatings

The stability of LbL multilayer coating is essential for biomedical materials application. The long-term stability of coating onto

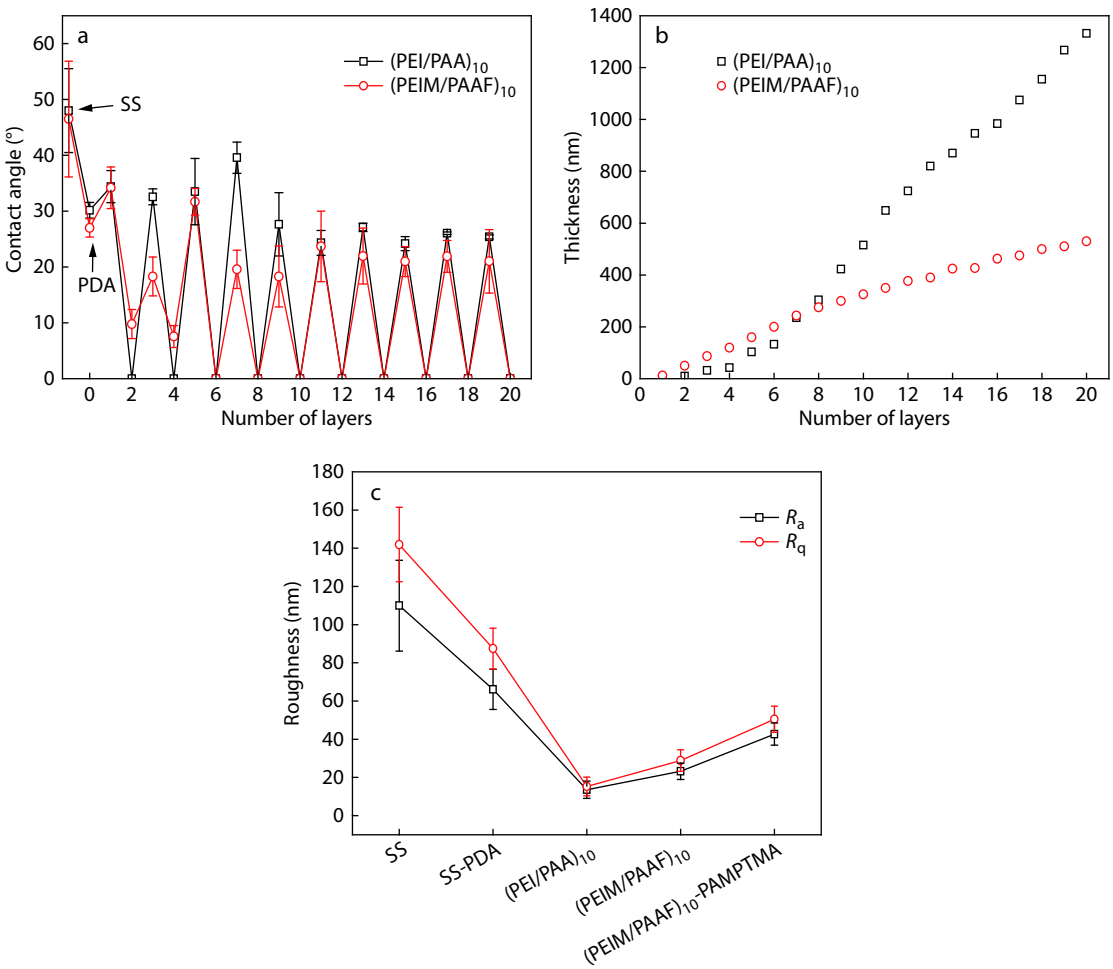

Fig. 4 (a) Water contact angles and sliding-angle changes of multilayer coatings $(PEI/PAA)_{10}$ and $(PEIM/PAAF)_{10}$ during 20 cycles; (b) Layer thickness change from QCM measurement for the formation of $(PEI/PAA)_{10}$ and $(PEIM/PAAF)_{10}$ multilayer; (c) Surface roughness of SS, SS-PDA and multilayer coatings resolved by AFM.

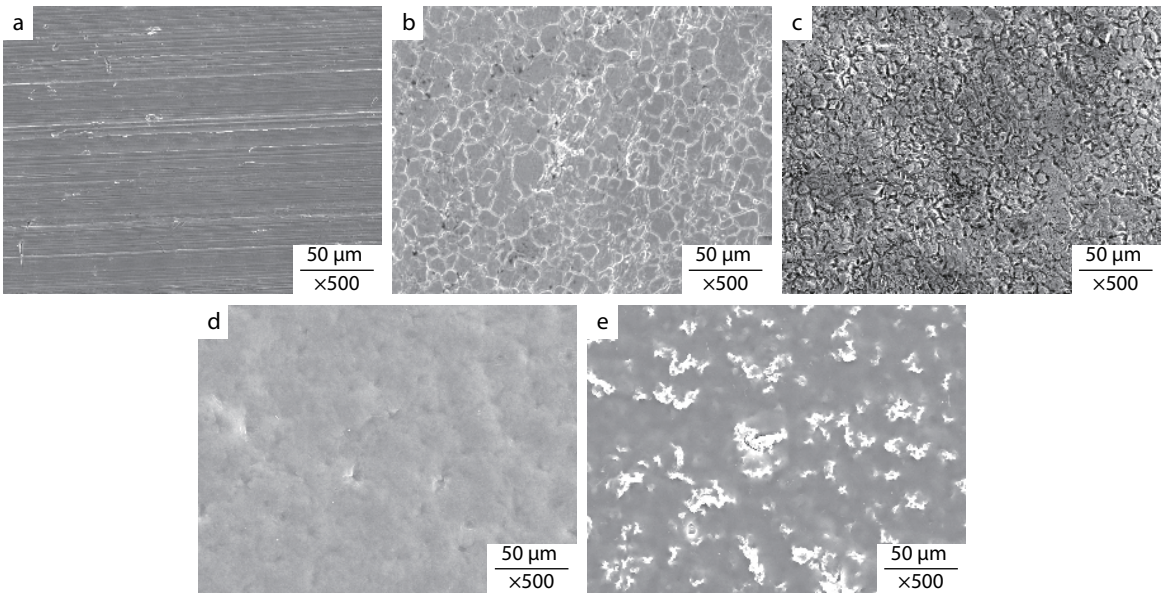

Fig. 5 FE-SEM images of (a) SS, (b) SS-PDA coating, (c) $(PEI/PAA)_{10}$ multilayer coating, (d) $(PEIM/PAAF)_{10}$ multilayer coating, and (e) $(PEIM/PAAF)_{10}$-PAMPTMA multilayer coating.

https://doi.org/10.1007/s10118-021-2513-3

the biomedical material surface could make the device durable in service. In Figs. 6(a)–6(c), the UV-vis spectra show the stability of multilayers coated onto quartz glass surface after being immersed in PBS (pH=7.4) solution for 5 days. The degradation ratios of multilayer coatings $(PEIM/PAAF)_{10}$ and $(PEIM/PAAF)_{10}$-PAMPTMA were slower than that of $(PEI/PAA)_{10}$. This is because the crosslinked multilayers not only contained noncovalent bonds (such as ionic and hydrogen bond), but also contained oxy-norbornene covalent bonds which were generated from Diels-Alder reaction between the positive layer and the negative layer. The surface nanoindentation characterization (Fig. 6d) also confirmed that the storage moduli of multilayer $(PEIM/PAAF)_{10}$ and $(PEIM/PAAF)_{10}$-PAMPTMA were higher than that of $(PEI/PAA)_{10}$ with increase of contact depth. Thus, the crosslinked multilayer coatings $(PEIM/PAAF)_{10}$ and $(PEIM/PAAF)_{10}$-PAMPTMA by LbL self-assembly and Diels-Alder reaction exhibited long-term anchoring onto the surface.

Self-healing Property of Multilayer Coatings

The ability to heal damage is critical to extending the service life of the antibacterial coating. A 5–10 μm wide crack, which exposed the underlying substrate, was made on the multilayer coatings $(PEI/PAA)_{10}$, $(PEIM/PAAF)_{10}$, and $(PEIM/PAAF)_{10}$-PAMPTMA with a scalpel, respectively. After the damaged coatings had been immersed in PBS, the crack of coating $(PEI/PAA)_{10}$ disappeared after 1 h, and the cracks of coatings $(PEIM/PAAF)_{10}$ and $(PEIM/PAAF)_{10}$-PAMPTMA disappeared after 1.5 h, indicating complete healing of the crack (Fig. 7).

The healing procedure of the multilayer coating $(PEI/PAA)_{10}$ was mainly ascribed to the dynamic nature of hydrogen bonds and the water absorption ability. When immersed in PBS, $(PEI/PAA)_{10}$ multilayer absorbed a large amount of PBS that can affect the hydrogen bonds between amide and carboxylic acid groups of PEI and PAA. Because the absorbed PBS acted as plasticizer to decrease the storage modulus of the multilayer and facilitated the mobility of PAA and PEI chains, the multilayer coating $(PEI/PAA)_{10}$ swelled and became soft and flowable, which enabled the fractured surfaces of the crack to come into intimate contact.[48] Next, the hydrogen-bonding interactions between PAA and PEI can be dynamically re-constructed in the fractured surfaces to heal the coating completely in 1 h when PBS was removed. However, it took 1.5 h for the self-healing procession of multilayer coatings $(PEIM/PAAF)_{10}$ and $(PEIM/PAAF)_{10}$-PAMPTMA onto SS-PDA slides. This is because the coatings were not only influenced by hydrogen bonds and PBS absorption ability but also the low flexible movement of polymer chains caused by Diels-Alder crosslinked reaction in the multilayer coatings. Moreover, $(PEIM/PAAF)_{10}$-PAMPTMA multilayer coating could undergo self-healing procedure under three cycles in Fig. S2 (in ESI).

Antibiofilm Assay *in Vitro*

Fig. 8 shows the *in vitro* antibiofilm activities of multilayer

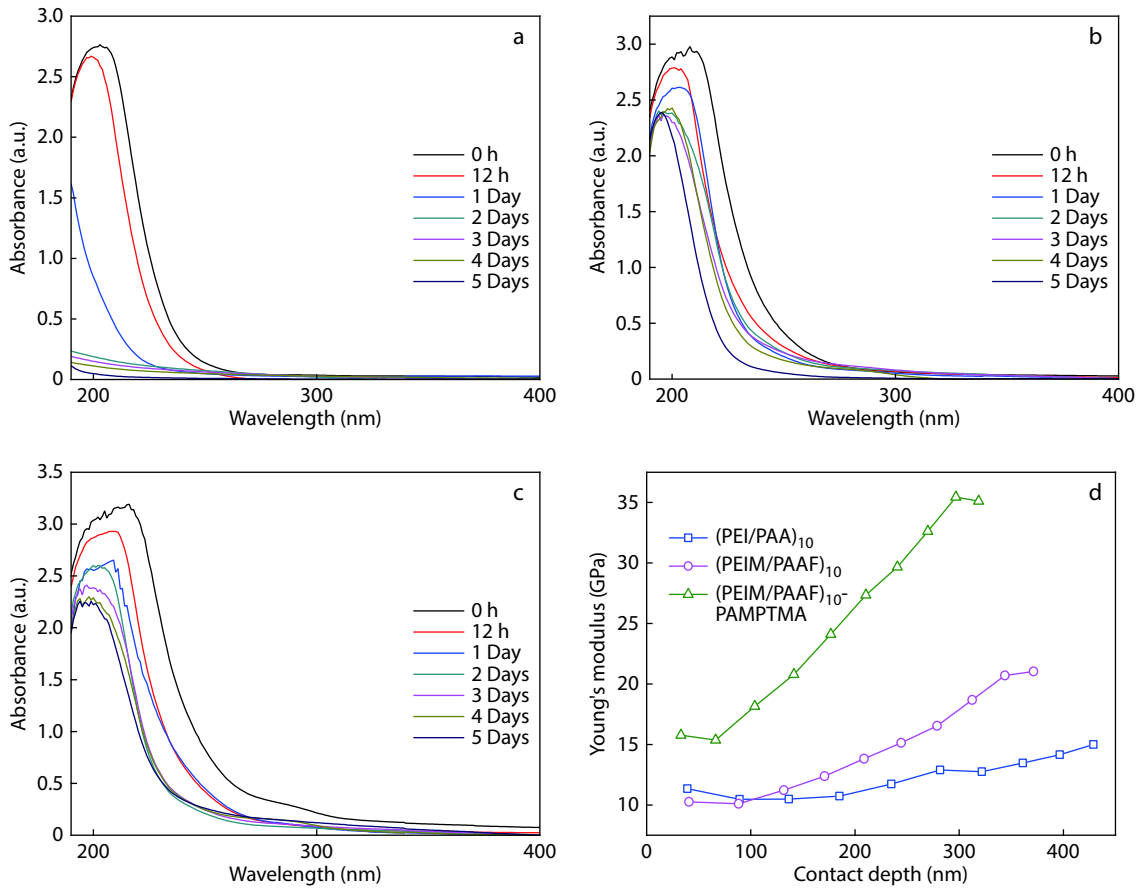

Fig. 6 UV-Vis spectra of multilayer coatings: (a) $(PEI/PAA)_{10}$, (b) $(PEIM/PAAF)_{10}$, (c) $(PEIM/PAAF)_{10}$-PAMPTMA; (d) Nanoindentation test.

https://doi.org/10.1007/s10118-021-2513-3

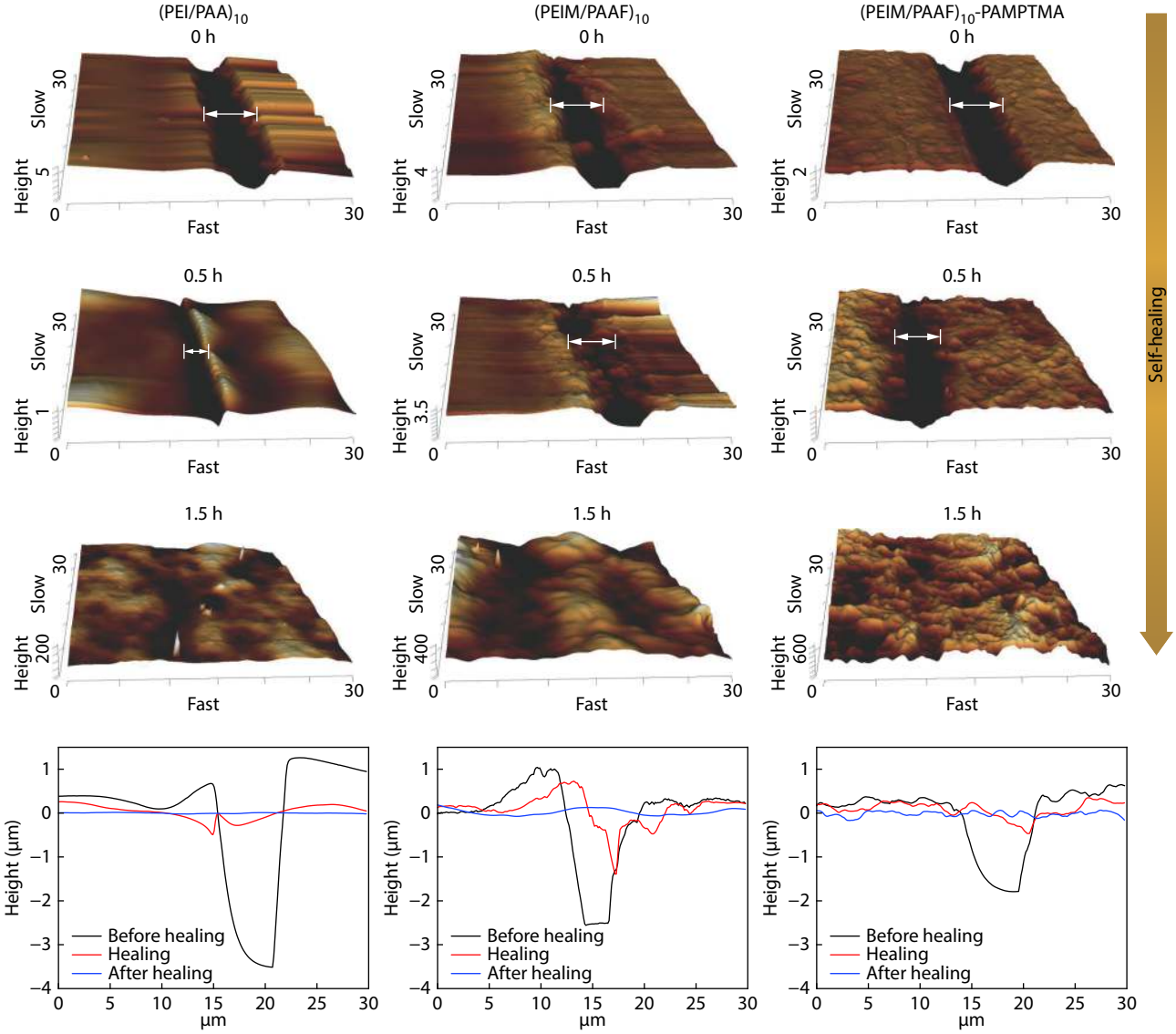

Fig. 7 Self-healing procession of multilayer coatings by AFM.

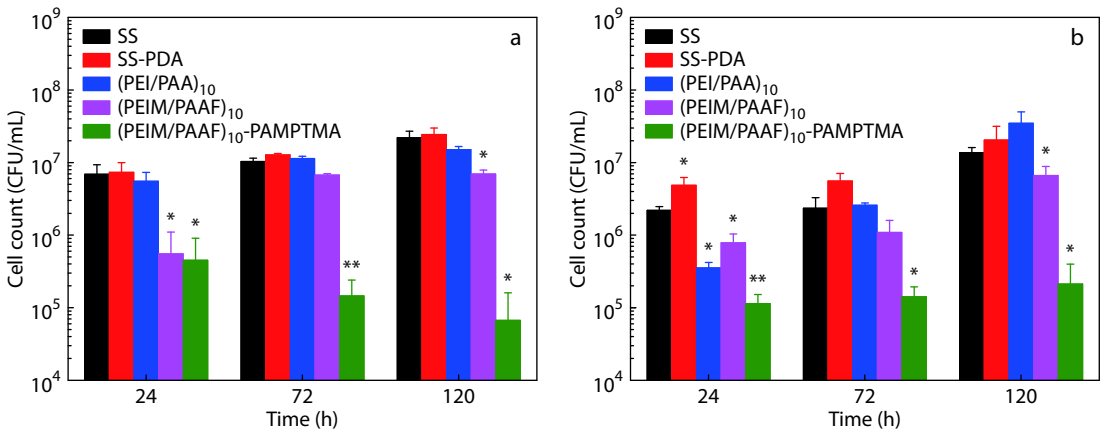

Fig. 8 Cell counts of biofilms grew in the presence (CFU) of multilayer coatings after different time periods: (a) *E. coli*, (b) *S. aureus*. * means $P<0.05$; ** means $P<0.01$; NS means not significant ($P>0.05$).

https://doi.org/10.1007/s10118-021-2513-3

coatings onto SS-PDA slide compared with unmodified SS slide. The cell counts of *E. coli* and *S. aureus* biofilms on the SS slide, SS-PDA slide and multilayer coating $(PEI/PAA)_{10}$ grew more rapidly than those of $(PEIM/PAAF)_{10}$ and $(PEIM/PAAF)_{10}$-PAMPTMA in 120 h. The biofilm grew on multilayer coatings $(PEIM/PAAF)_{10}$ and $(PEIM/PAAF)_{10}$-PAMPTMA surfaces relatively slowly as compared with other samples. Especially $(PEIM/PAAF)_{10}$-PAMPTMA coating obviously showed antibiofilm and contact killing effect against the bacteria, with the log reduction of 1.69 (killing ratio 97.9%) for *E. coli* and 1.59 (killing ration 97.4%) for *S. aureus* in 120 h, respectively.

To further explain the antibiofilm mechanism of surface coating, we compared the antibiofilm property of SS and modified SS slides in micromorphology. In Fig. 9, thick and dense *E. coli* and *S. aureus* biofilms attached onto the SS slide and SS-PDA surfaces from the bacterial live/dead fluorescence and FE-SEM images. This is attributed to their relatively hydrophobic and anionic surface. Though the multilayer coating $(PEI/PAA)_{10}$ was hydrophilic, the noncovalent bond LbL self-assembled multilayer was not stable and could be detached from the SS-PDA slide in 120 h (5 days), leading to the formation of *E. coli* and *S. aureus* biofilms on the SS-PDA surface. While the crosslinked multilayer coating $(PEIM/PAAF)_{10}$ onto SS-PDA slide had stable coating, it could only repel the

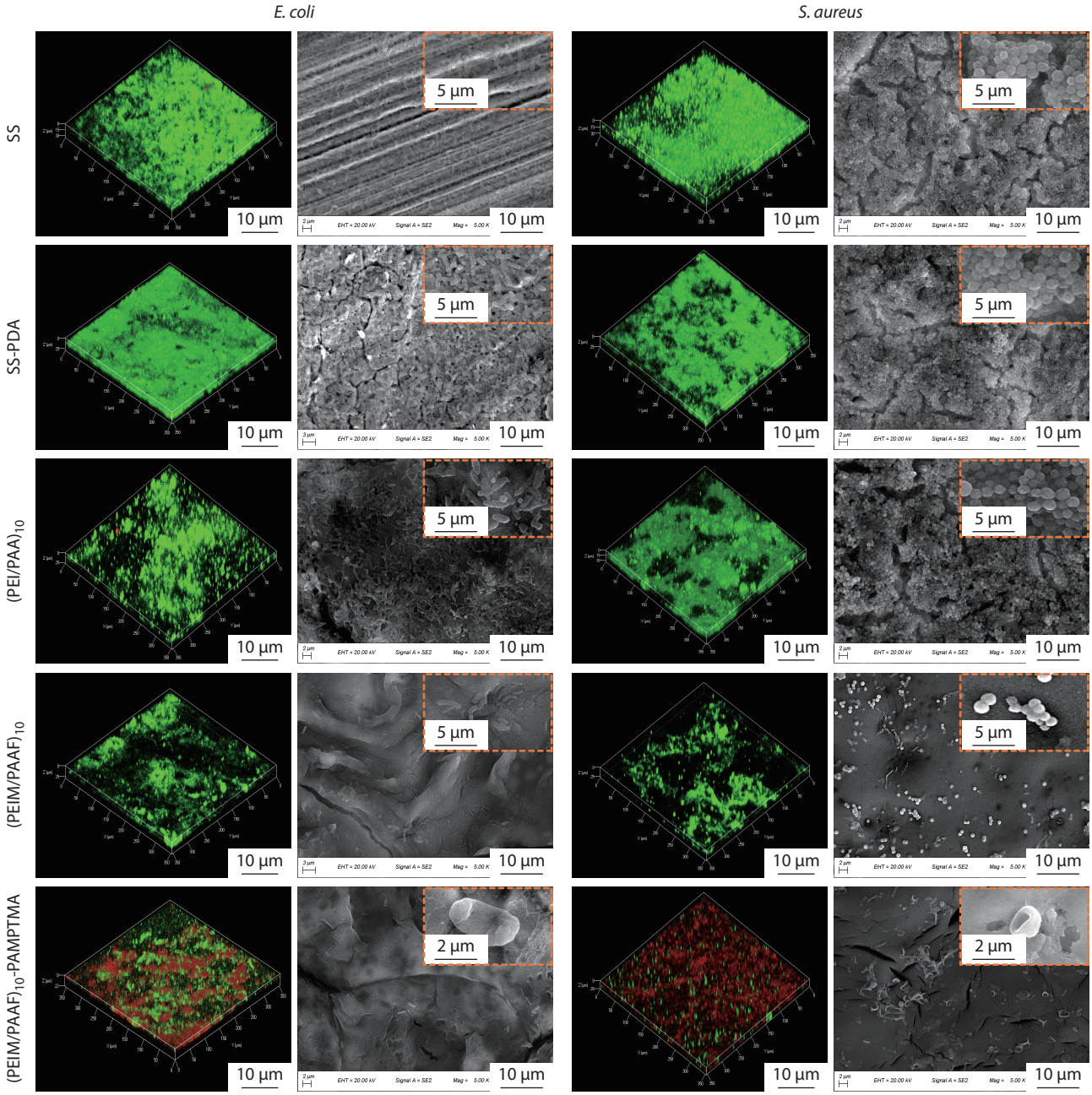

Fig. 9 Live/dead fluorescence and FE-SEM images of *E. coli* and *S. aureus* on SS slide, SS-PDA, and multilayer coatings after 120 h (the red dash lines represented magnified of biofilms).

https://doi.org/10.1007/s10118-021-2513-3

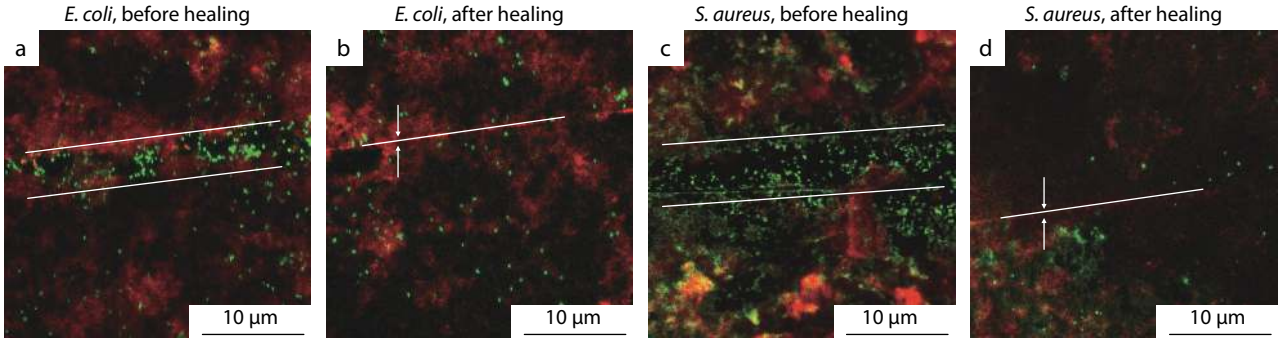

Fig. 10 Live/dead fluorescence of multilayer coating $(PEIM/PAAF)_{10}$-PAMPTMA: before healing for (a) *E. coli* and (c) *S. aureus*, after healing for (b) *E. coli* and (d) *S. aureus*.

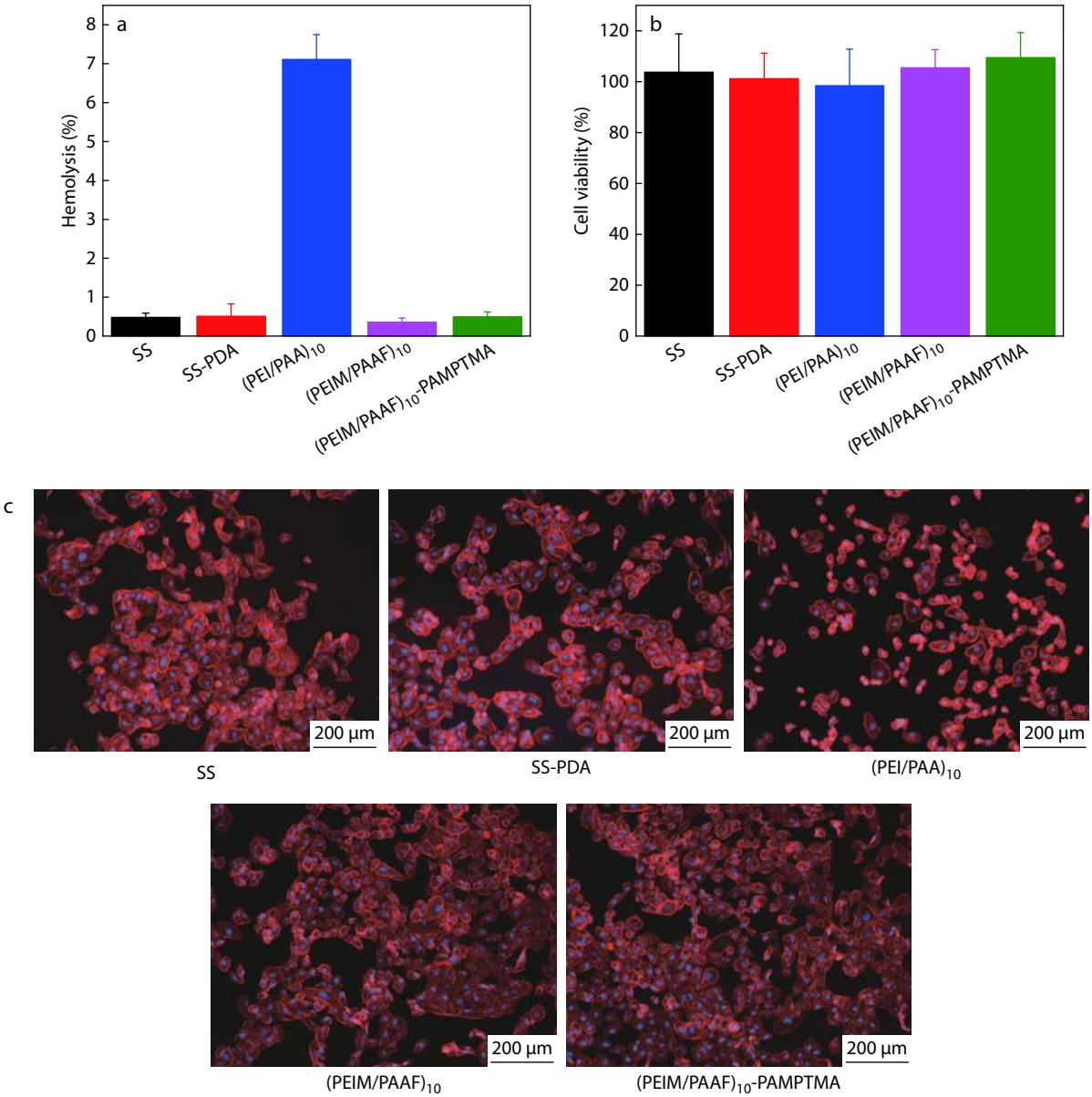

Fig. 11 (a) Hemolysis and (b) MTT assay of the cell viability for the multilayer coatings onto SS slide; (c) Fluorescent images of MC3T3-E1 and stained with rhodamine phalloidin.

https://doi.org/10.1007/s10118-021-2513-3

bacteria from the coating surface due to the negative surface zeta potential and electrostatic repulsion.[49] There were few *E. coli* and *S. aureus* biofilms attached onto the $(PEIM/PAAF)_{10}$-PAMPTMA coating after 120 h and dead bacteria on the surface (killing ratio 97.9% for *E. coli* and 97.4% for *S. aureus*, respectively), because PAMPTMA was a strong cationic polymer which had low minimum inhibitory concentrations (MIC) for both *E. coli* and *S. aureus*,[50] and made the surface zeta potential of the multilayer coating change into positive.

To further investigate surface antibiofilm property of the healed $(PEIM/PAAF)_{10}$-PAMPTMA coating, the $(PEIM/PAAF)_{10}$-PAMPTMA coating damaged with a ~5 μm wide crack and the healed $(PEIM/PAAF)_{10}$-PAMPTMA coating were incubated with *E. coli* and *S. aureus* for 6 h, respectively. Figs. 10(a) and 10(c) show that a large amount of *E. coli* and *S. aureus* appeared on the crack area of the damaged coating. No obvious *E. coli* or *S. aureus* appeared on the healed regions of the coating in Figs. 10(b) and 10(d). Therefore, the healed $(PEIM/PAAF)_{10}$-PAMPTMA coating could restore its antibiofilm function in a short time.

Hemolytic Activity and Cytocompatibility Assay *in Vitro* of Multilayer Coatings

Fig. 11(a) shows the hemolysis of unmodified and modified SS slides. The hemolysis of SS slide, SS-PDA, $(PEIM/PAAF)_{10}$, and $(PEIM/PAAF)_{10}$-PAMPTMA coating was about 0.5%, which means nonhemolytic for biomaterials according to the American Society for Testing and Materials (ASTM) F756-00 standard (less than 2%).[51] The hemolysis of $(PEI/PAA)_{10}$ was the highest (7%), because there was no covalent bond crosslinking in the multilayer. PEI layers and PAA layers detached from the SS slide surface and as a result, PEI layers could make the blood cell break. To evaluate the potential cytotoxicity of multilayer coatings, the MC3T3-E1 cells with the extracted liquid of each sample were immersed in the culture medium and measured by MTT testing. After 24 h incubation with samples, the MC3T3-E1 cell viability was all above 95% (Figs. 11b and 11c) and was not significantly different from that of SS slide. Thus, surface LbL multilayer coatings were non-cytotoxic.

In Vivo Antimicrobial Activity of Crosslinked Multilayer Coating

The *in vivo* experiments were performed on mice after subcutaneous implantation of the slides seeded respectively with *E. coli* and *S. aureus* to evaluate the antimicrobial ability of multilayer coating $(PEIM/PAAF)_{10}$-PAMPTMA in a real biosystem. *E. coli* (10 μL of 10^6 CFU/mL) and *S. aureus* (10 μL of 10^6 CFU/mL) were respectively spotted on the SS slide (d=5 mm) or

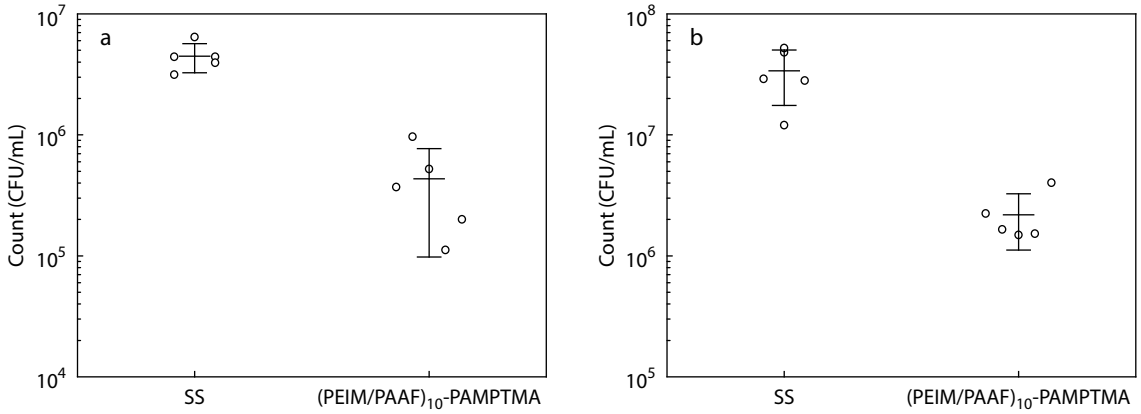

Fig. 12 *In vivo* essay of CFU of coatings biofilm after 120 h: (a) *E. coli* (P<0.01), (b) *S. aureus* (P<0.01).

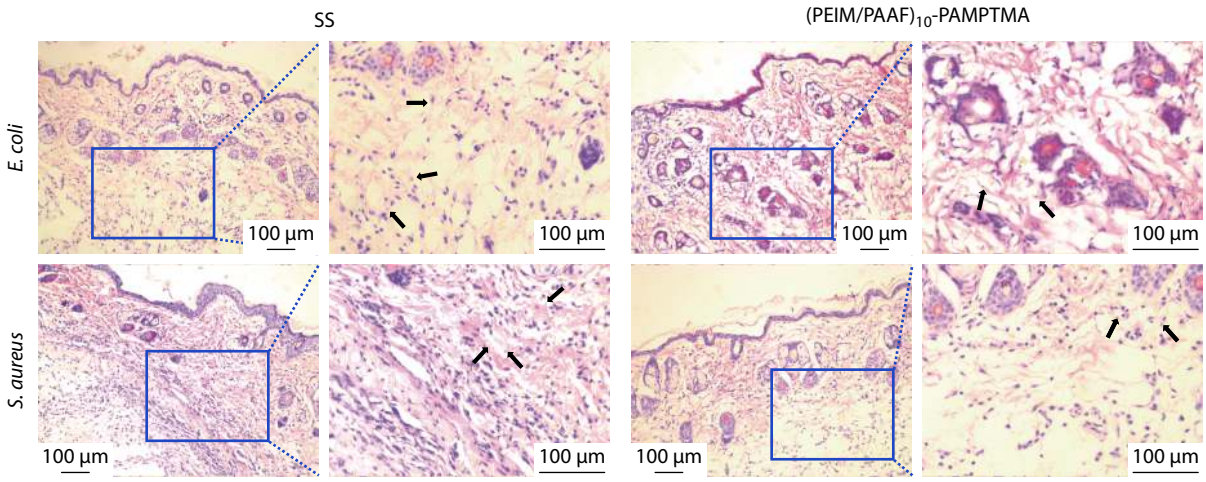

Fig. 13 Histological sections from SS slide and SS coated with $(PEIM/PAAF)_{10}$-PAMPTMA stained by H&E assay after 120 h.

https://doi.org/10.1007/s10118-021-2513-3

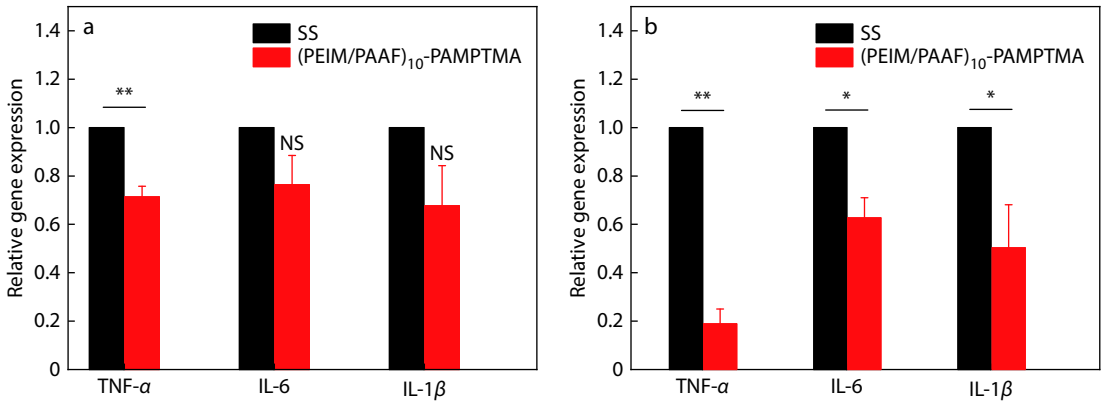

Fig. 14 Relative gene expression in local anti-infection skin tissue at 120 h after surgery measured to evaluate the level of inflammation (TNF-*α*, IL-6, and IL-1*β*) in each group: (a) *E. coli*, (b) *S. aureus*.

multilayer coating $(PEIM/PAAF)_{10}$-PAMPTMA on SS-PDA (*d*= 5 mm) and dried for 15 min. The slide was implanted into each incision of mice's back respectively for 120 h culture. As seen from Figs. 12(a) and 12(b), the log reduction of multilayer coating $(PEIM/PAAF)_{10}$-PAMPTMA onto SS-PDA slide for *E. coli* was 1.01 (killing ratio 90.3%), while the log reduction of the multilayer coating for *S. aureus* was 1.19 (killing ratio 93.5%) after 120 h, which was consistent with the *in vitro* results.

In Vivo Anti-inflammation Evaluation

The skin tissues around the implantation were sectioned and stained by hematoxylin and eosin for histological evaluation (Fig. 13). A lot of inflammatory cells (stained by the blue color of arrow area) were visible in the tissue from SS slide, demonstrating serious infection by *E. coli* and *S. aureus*, respectively. However, there were few inflammatory cells visible in the tissue from multilayer coating $(PEIM/PAAF)_{10}$-PAMPTMA onto SS-PDA slide infected by *E. coil* and *S. aureus*, respectively. The mechanism of anti-inflammation of the multilayer coating would be further investigated. In Figs. 14(a) and 14(b), by extracting the RNA from local skin tissue, we found that proinflammation related genes like TNF-*α*, IL-6, and IL-1*β*[52] as shown were more significantly down-regulated in SS-PDA slide coated with $(PEIM/PAAF)_{10}$-PAMPTMA for *S. aureus* than that for *E. coli*. Consistent with histological study, it is worth noting that the multilayer coating $(PEIM/PAAF)_{10}$-PAMPTMA had good effect on anti-inflammation, which could significantly avoid the risk of biomedical implants from microbial contamination.

CONCLUSIONS

Herein, we reported robust and self-healable antibiofilm surface coatings *via* LbL self-assembly and Diels-Alder reaction. The surface structure and physical properties of the coatings were confirmed by XPS, water contact angle, QCM, UV-Vis spectra, nanoindentation and AFM. The multilayer coating $(PEIM/PAAF)_{10}$-PAMPTMA obtained by the crosslinked LbL self-assembly exhibited unique stability and self-healability. *In vitro* data of the multilayer coating indicated obvious long-term antibiofilm property; a log reduction for *E. coli* was 1.69 (killing ratio 97.9%) and for *S. aureus* was 1.59 (killing ration 97.4%) in 120 h. Furthermore, the multilayer coating also inhibited the growth of *E. coli* and *S. aureus* biofilms after the crack healed. $(PEIM/PAAF)_{10}$-PAMPTMA coating also exhibited low hemolysis and high cell viability. The *in vivo* assay confirmed that the multilayer coating exhibited not only excellent antibiofilm effect (log reduction of 1.01 for *E. coli*. and 1.19 for *S. aureus* in 120 h), but also good efficacy on inflammation suppression. All these results revealed that the self-healable antibiofilm coating was a promising strategy for bacterial infection control of various implants in practical applications.

Electronic Supplementary Information

Electronic supplementary information (ESI) is available free of charge in the online version of this article at https://doi.org/10.1007/s10118-021-2513-3.

ACKNOWLEDGMENTS

This work was financially supported by the Natural Science Foundation of Jiangsu Province (No. BK20180963) and the Natural Science Foundation of the Jiangsu Higher Education Institutions of China (No. 19KJD430001).

REFERENCES

1 Ding, X. K.; Duan, S.; Ding, X. J.; Liu, R. H.; Xu, F. J. Versatile antibacterial materials: an emerging arsenal for combatting bacterial pathogens. *Adv. Funct. Mater.* **2018**, *28*, 19.
2 Li, C.; Lu, D. Y.; Deng, J. J.; Zhang, X.; Yang, P. Amyloid-like rapid surface modification for antifouling and in-depth remineralization of dentine tubules to treat dental hypersensitivity. *Adv. Mater.* **2019**, *31*, 1903973.
3 Zhao, J.; Qu, Y.; Chen, H.; Xu, R.; Yu, Q.; Yang, P. Self-assembled proteinaceous wound dressings attenuate secondary trauma and improve wound healing *in vivo*. *J. Mater. Chem. B* **2018**, *6*, 4645–4655.
4 Kang, T.; Banquy, X.; Heo, J.; Lim, C.; Lynd, N. A.; Lundberg, P.; Oh, D. X.; Lee, H. K.; Hong, Y. K.; Hwang, D. S.; Waite, J. H.; Israelachvili, J. N.; Hawker, C. J. Mussel-inspired anchoring of polymer loops that provide superior surface lubrication and antifouling properties. *ACS Nano* **2016**, *10*, 930–937.
5 Baggerman, J.; Smulders, M. M. J.; Zuilhof, H. Romantic surfaces: a systematic overview of stable, biospecific, and antifouling

zwitterionic surfaces. *Langmuir* **2019**, *35*, 1072–1084.
6 Zhang, R.; Zhang, L.; Tian, N.; Ma, S.; Liu, Y.; Yu, B.; Pei, X.; Zhou, F. The tethered fibrillar hydrogels brushes for underwater antifouling. *Adv. Mater. Interfaces* **2017**, *4*, 1601039.
7 Hu, X.; Tian, J.; Li, C.; Su, H.; Qin, R.; Wang, Y.; Cao, X.; Yang, P. Amyloid-like protein aggregates: a new class of bioinspired materials merging an interfacial anchor with antifouling. *Adv. Mater.* **2020**, *32*, 2000128.
8 Yang, W.; Zhao, W.; Liu, Y.; Hu, H.; Pei, X.; Wu, Y.; Zhou, F. The effect of wetting property on anti-fouling/foul-release performance under quasi-static/hydrodynamic conditions. *Prog. Org. Coat.* **2016**, *95*, 64–71.
9 Borjihan, Q.; Yang, J.; Song, Q.; Gao, L.; Xu, M.; Gao, T.; Liu, W.; Li, P.; Li, Q.; Dong, A. Povidone-iodine-functionalized fluorinated copolymers with dual-functional antibacterial and antifouling activities. *Biomater. Sci.* **2019**, *7*, 3334–3347.
10 Wu, J.; Yu, C.; Li, Q. Novel regenerable antimicrobial nanocomposite membranes: effect of silver loading and valence state. *J. Membr. Sci.* **2017**, *531*, 68–76.
11 Mitra, D.; Li, M.; Kang, E. T.; Neoh, K. G. Transparent copper-based antibacterial coatings with enhanced efficacy against *Pseudomonas aeruginosa*. *ACS Appl. Mater. Interfaces* **2019**, *11*, 73–83.
12 Xu, L. C.; Meyerhoff, M. E.; Siedlecki, C. A. Blood coagulation response and bacterial adhesion to biomimetic polyurethane biomaterials prepared with surface texturing and nitric oxide release. *Acta Biomater.* **2019**, *84*, 77–87.
13 Zeng, Q.; Zhu, Y.; Yu, B.; Sun, Y.; Ding, X.; Xu, C.; Wu, Y. W.; Tang, Z.; Xu, F. J. Antimicrobial and antifouling polymeric agents for surface functionalization of medical implants. *Biomacromolecules* **2018**, *19*, 2805–2811.
14 Siedenbiedel, F.; Tiller, J. C. Antimicrobial polymers in solution and on surfaces: overview and functional principles. *Polymers* **2012**, *4*, 46–71.
15 Zhou, C.; Song, H.; Loh, J. L. C.; She, J.; Deng, L.; Liu, B. Grafting antibiofilm polymer hydrogel film onto catheter by SARA SI-ATRP. *J. Biomater. Sci., Polym. Ed.* **2018**, *29*, 2106–2123.
16 Atefyekta, S.; Pihl, M.; Lindsay, C.; Heilshorn, S. C.; Andersson, M. Antibiofilm elastin-like polypeptide coatings: functionality, stability, and selectivity. *Acta Biomater.* **2019**, *83*, 245–256.
17 Gu, J.; Su, Y. J.; Liu, P.; Li, P.; Yang, P. An environmentally benign antimicrobial coating based on a protein supramolecular assembly. *ACS Appl. Mater. Interfaces* **2017**, *9*, 198–210.
18 Wang, M.; Shi, J.; Mao, H.; Sun, Z.; Guo, S.; Guo, J.; Yan, F. Fluorescent imidazolium-type poly(ionic liquid)s for bacterial imaging and biofilm inhibition. *Biomacromolecules* **2019**, *20*, 3161–3170.
19 Yang, W. J.; Tao, X.; Zhao, T. T.; Weng, L. X.; Kang, E. T.; Wang, L. H. Antifouling and antibacterial hydrogel coatings with self-healing properties based on a dynamic disulfide exchange reaction. *Polym. Chem.* **2015**, *6*, 7027–7035.
20 Wei, T.; Tang, Z.; Yu, Q.; Chen, H. Smart antibacterial surfaces with switchable bacteria-killing and bacteria-releasing capabilities. *ACS Appl. Mater. Interfaces* **2017**, *9*, 37511–37523.
21 Tian, J.; Liu, Y.; Miao, S.; Yang, Q.; Hu, X.; Han, Q.; Xue, L.; Yang, P. Amyloid-like protein aggregates combining antifouling with antibacterial activity. *Biomater. Sci.* **2020**.
22 Wang, Z. H.; Fei, G. X.; Xia, H. S.; Zuilhof, H. Dual water-healable zwitterionic polymer coatings for anti-biofouling surfaces. *J. Mater. Chem. B* **2018**, *6*, 6930–6935.
23 Yuan, P.; Qiu, X.; Wang, X.; Tian, R.; Wang, L.; Bai, Y.; Liu, S.; Chen, X. Substrate-independent coating with persistent and stable antifouling and antibacterial activities to reduce bacterial infection for various implants. *Adv. Healthc. Mater.* **2019**, *8*, e1801423.
24 Wang, Q.; Wang, L.; Gao, L.; Yu, L.; Feng, W.; Liu, N.; Xu, M.; Li, X.; Li, P.; Huang, W. Stable and self-healable LbL coating with antibiofilm efficacy based on alkylated polyethyleneimine micelles. *J. Mater. Chem. B* **2019**, *7*, 3865–3875.
25 Wei, Z.; Yang, J. H.; Zhou, J.; Xu, F.; Zrínyi, M.; Dussault, P. H.; Osada, Y.; Chen, Y. M. Self-healing gels based on constitutional dynamic chemistry and their potential applications. *Chem. Soc. Rev.* **2014**, *43*, 8114–8131.
26 Hillewaere, X. K. D.; Du Prez, F. E. Fifteen chemistries for autonomous external self-healing polymers and composites. *Prog. Polym. Sci.* **2015**, *49-50*, 121–153.
27 Jin, J.; Cai, L.; Jia, Y. G.; Liu, S.; Chen, Y.; Ren, L. Progress in self-healing hydrogels assembled by host-guest interactions: preparation and biomedical applications. *J. Mater. Chem. B* **2019**, *7*, 1637–1651.
28 Yang, Q. M.; Liu, Y. C.; Chen, L. X.; Yang, P. Study on the amyloid-like fibrinogen-based Nanofilm. *Acta Polymerica Sinica* (in Chinese) **2020**, *51*, 890–900.
29 Fan, F.; Zhou, C.; Wang, X.; Szpunar, J. Layer-by-Layer assembly of a self-healing anticorrosion coating on magnesium alloys. *ACS Appl. Mater. Interfaces* **2015**, *7*, 27271–27278.
30 Zhang, X.; Xu, Y.; Zhang, X.; Wu, H.; Shen, J.; Chen, R.; Xiong, Y.; Li, J.; Guo, S. Progress on the layer-by-layer assembly of multilayered polymer composites: strategy, structural control and applications. *Prog. Polym. Sci.* **2019**, *89*, 76–107.
31 Zhu, X. Y.; Loh, X. J. Layer-by-layer assemblies for antibacterial applications. *Biomater. Sci.* **2015**, *3*, 1505–1518.
32 Wei, T.; Zhan, W. J.; Cao, L. M.; Hu, C. M.; Qu, Y. C.; Yu, Q.; Chen, H. Multifunctional and regenerable antibacterial surfaces fabricated by a universal strategy. *ACS Appl. Mater. Interfaces* **2016**, *8*, 30048–30057.
33 Wang, B. L.; Ren, K. F.; Chang, H.; Wang, J. L.; Ji, J. Construction of degradable multilayer films for enhanced antibacterial properties. *ACS Appl. Mater. Interfaces* **2013**, *5*, 4136–4143.
34 Zhu, X.; Guo, S.; Janczewski, D.; Velandia, F. J.; Teo, S. L.; Vancso, G. J. Multilayers of fluorinated amphiphilic polyions for marine fouling prevention. *Langmuir* **2014**, *30*, 288–296.
35 Min, H.; Qian, W.; Zhao, W.; Zhao, C. S. Substrate-independent ultrathin hydrogel film as antifouling and antibacterial layer for microfiltration membrane anchored *via* layer-by-layer thiol-ene "click" reaction. *J. Mater. Chem. B* **2018**, *6*, 3904–3913.
36 Cai, T.; Li, M.; Neoh, K. G.; Kang, E. T. Preparation of stimuli responsive polycaprolactone membranes of controllable porous morphology *via* combined atom transfer radical polymerization, ring-opening polymerization and thiol-yne click chemistry. *J. Mater. Chem.* **2012**, *22*, 16248–16258.
37 Song, H. Y.; Ngai, M. H.; Song, Z. Y.; MacAry, P. A.; Hobley, J.; Lear, M. J. Practical synthesis of maleimides and coumarin-linked probes for protein and antibody labelling *via* reduction of native disulfides. *Org. Biomol. Chem.* **2009**, *7*, 3400–3406.
38 Chen, X. C.; Ren, K. F.; Zhang, J. H.; Li, D. D.; Zhao, E.; Zhao, Z. J.; Xu, Z. K.; Ji, J. Humidity-triggered self-healing of microporous polyelectrolyte multilayer coatings for hydrophobic drug delivery. *Adv. Funct. Mater.* **2015**, *25*, 7470–7477.
39 Abreu, C. M. R.; Mendonça, P. V.; Serra, A. C.; Popov, A. V.; Matyjaszewski, K.; Guliashvili, T.; Coelho, J. F. J. Inorganic sulfites: efficient reducing agents and supplemental activators for atom transfer radical polymerization. *ACS Macro Lett.* **2012**, *1*, 1308–1311.
40 Mendonça, P. V.; Konkolewicz, D.; Averick, S. E.; Serra, A. C.; Popov, A. V.; Guliashvili, T.; Matyjaszewski, K.; Coelho, J. F. J. Synthesis of cationic poly((3-acrylamidopropyl)trimethyl-ammonium chloride) by SARA ATRP in ecofriendly solvent mixtures. *Polym. Chem.* **2014**, *5*, 5829–5836.
41 Chen, X. C.; Huang, W. P.; Ren, K. F.; Ji, J. Self-healing label

materials based on photo-cross-linkable polymeric films with dynamic surface structures. *ACS Nano* **2018**, *12*, 8686–8696.
42 Chen, D.; Wu, M.; Li, B.; Ren, K.; Cheng, Z.; Ji, J.; Li, Y.; Sun, J. Layer-by-layer-assembled healable antifouling films. *Adv. Mater.* **2015**, *27*, 5882–5888.
43 Liu, Y. L.; Lee, H. C. Preparation and properties of polyhedral oligosilsequioxane tethered aromatic polyamide nanocomposites through Michael addition between maleimide-containing polyamides and an amino-functionalized polyhedral oligosilsequioxane. *J. Polym. Sci., Part A: Polym. Chem.* **2006**, *44*, 4632–4643.
44 Asha, A. B.; Chen, Y.; Zhang, H.; Ghaemi, S.; Ishihara, K.; Liu, Y.; Narain, R. Rapid mussel-inspired surface zwitteration for enhanced antifouling and antibacterial properties. *Langmuir* **2018**, *35*, 1621–1630.
45 Surman, F.; Riedel, T.; Bruns, M.; Kostina, N. Y.; Sedlakova, Z.; Rodriguez-Emmenegger, C. Polymer brushes interfacing blood as a route toward high performance blood contacting devices. *Macromol. Biosci.* **2015**, *15*, 636–646.
46 Hänni-Ciunel, K.; Findenegg, G. H.; von Klitzing, R. Water contact angle on polyelectrolyte-coated surfaces: effects of film swelling and droplet evaporation. *Soft Mater.* **2007**, *5*, 61–73.
47 DeLongchamp, D. M.; Hammond, P. T. Highly ion conductive poly(ethylene oxide)-based solid polymer electrolytes from hydrogen bonding layer-by-layer assembly. *Langmuir* **2004**, *20*, 5403–5411.
48 Li, Y. X.; Pan, T. Z.; Ma, B. H.; Liu, J. Q.; Sun, J. Q. Healable antifouling films composed of partially hydrolyzed poly(2-ethyl-2-oxazoline) and poly(acrylic acid). *ACS Appl. Mater. Interfaces* **2017**, *9*, 14429–14436.
49 Bazaka, K.; Jacob, M. V.; Chrzanowski, W.; Ostrikov, K. Anti-bacterial surfaces: natural agents, mechanisms of action, and plasma surface modification. *RSC Adv.* **2015**, *5*, 48739–48759.
50 Chin, W.; Zhong, G.; Pu, Q.; Yang, C.; Lou, W.; De Sessions, P. F.; Periaswamy, B.; Lee, A.; Liang, Z. C.; Ding, X.; Gao, S.; Chu, C. W.; Bianco, S.; Bao, C.; Tong, Y. W.; Fan, W.; Wu, M.; Hedrick, J. L.; Yang, Y. Y. A macromolecular approach to eradicate multidrug resistant bacterial infections while mitigating drug resistance onset. *Nat. Commun.* **2018**, *9*.
51 Bauer, M.; Lautenschlaeger, C.; Kempe, K.; Tauhardt, L.; Schubert, U. S.; Fischer, D. Poly(2-ethyl-2-oxazoline) as alternative for the stealth polymer poly(ethylene glycol): comparison of *in vitro* cytotoxicity and hemocompatibility. *Macromol. Biosci.* **2012**, *12*, 986–998.
52 Xu, M.; Khan, A.; Wang, T.; Song, Q.; Han, C.; Wang, Q.; Gao, L.; Huang, X.; Li, P.; Huang, W. Mussel-inspired hydrogel with potent *in vivo* contact-active antimicrobial and wound healing promoting activities. *ACS Appl. Bio. Mater.* **2019**, *2*, 3329–3340.

https://doi.org/10.1007/s10118-021-2513-3